

## Galaxy Cluster Weak Lensing in the Radio

ANDI GRAY,<sup>1,2</sup> MARK LACY,<sup>1</sup> AND WIPHU RUJOPAKARN<sup>3</sup>

<sup>1</sup>*National Radio Astronomy Observatory, 520 Edgemont Road, Charlottesville, VA 22903, USA*

<sup>2</sup>*Tufts University, Department of Physics & Astronomy  
574 Boston Avenue, Medford, MA 02155, USA*

<sup>3</sup>*Chulalongkorn University, Department of Physics, 254 Phayathai Road, Bangkok, Pathum Wan 10330, Thailand*

### ABSTRACT

We present steps towards the first significant measurement of galaxy cluster-driven weak lensing using only radio data. This work employed a stacked catalog of cluster images, in an attempt to mitigate noise domination from low source-density in any single radio image. At this stage, we report a mass estimate for the cluster stack of  $8.405 \pm 1.092 \times 10^{14} [M_{\odot}]$  at  $1.68 \pm 0.22\sigma$ . However, we believe our initial bootstrapped significance analysis likely underestimated this confidence value, especially given the clear strength and profile of the lensing signal. Our progress is discussed in the context of established work in the optical, as well as existing methods involving radio input. Additionally, we motivate the advantages of including radio observations in weak lensing work, highlighting upcoming relevant surveys and science instruments. Finally, we comment on coming improvements to this work.

*Keywords:* gravitational lensing: weak – methods: statistical – radio continuum: galaxies – cosmology: observations

### 1. INTRODUCTION

Gravitational lensing, particularly in the weak regime, has become ubiquitous as a tool for probing unseen dark matter distributions (e.g. Oguri et al. (2010)), unraveling tangled galaxy evolution histories (e.g. Taylor et al. (2020)), and in mining precision cosmological parameters (e.g. KiDS-1000 Heymans et al. (2021); DES-3yr Abbott et al. (2021)); among any number of other astrophysical applications. Much of this existing body of work has been performed using optical or near-infrared (NIR) observations. However, there has been interest in the applicability of radio data to lensing studies; with some examples being Chang et al. (2004) presenting the first use of a radio survey for cosmic shear measurements, and Demetroullas & Brown (2017) combining SDSS optical and VLA-FIRST radio data to produce significant results on galaxy-galaxy and galaxy-cluster lensing. To our knowledge though, smaller-scale studies of weak lensing have yet to be successful with only radio data. Overcoming this barrier is the main goal of this work.

Employing radio data to extract weak lensing measurements presents a few compelling advantages. Weak lensing analyses generally rely on a statistical search for a systematic signal (significant alignment of background galaxy shapes relative to the lensing-driver) (e.g. Seitz & Schneider 1995). The primary foothold to this end is to assume that the distribution of *intrinsic* (unlensed) galaxy ellipticities must be random, which cannot account for any inherent environmental or other fundamental galaxy organization. However, if any information on the intrinsic alignment of the galaxy is available that is not affected by lensing, then this can be used to improve the accuracy of the mass reconstruction. For example, with radio polarimetry data, it would be feasible to estimate the intrinsic galaxy shape alignment directly using the fact that for a generic spiral galaxy the polarization should point up/down out of its main plane (Stil et al. 2009). This lead Brown & Battye (2011) to suggest that polarization measurements could significantly improve the accuracy of weak lensing measurements. Similarly, using radio spectral line maps, we can track the overall location and movement of gas (e.g. HI) in the galaxy to infer the major axis of rotation (Wright 1974). Blain (2002) and Morales (2006) showed that this information could also improve weak lensing estimates.

A more well-developed motive for including radio data in weak lensing work concerns systematics. Battye et al. (2020) (SuperCLASS survey design), Harrison et al. (2020) (DR1), and references therein discuss how radio interferometer

Name	Right Ascension (RA) (deg)	Declination (Dec) (deg)	Redshift ( $z$ )
WARP J1226.9+3332	186.741667	33.548361	0.890
Abell 851	145.741667	46.986667	0.407
Abell 2813	10.851667	-20.621389	0.292
Abell 3088	46.767083	-28.673333	0.253
MACS J0032.1+1808	8.046583	18.130556	0.389
Abell 611	120.236667	36.236111	0.288
MACS J2252.9-2133	343.223708	-21.567444	-
MACS J0111.5+0856	17.891542	8.935167	0.263
MACS J0455.2+0659	73.816917	6.990417	-
MACS J0600.2-2008	90.072083	-20.136389	-
MACS J1314.4-2515	198.606958	-25.254306	0.247
MACS J1731.7+2252	262.927167	22.879444	0.361

**Table 1.** Name and basic pointing information for the twelve galaxy clusters used in this study.

and optical aperture, CCD systematics should be uncorrelated in lensing measurements, such that teaming the two datasets together could reduce error ranges down to just the inherent statistical uncertainty. This approach is one of the main facets of the SuperCLASS survey, which combines Subaru Suprime-Cam optical with *e*-MERLIN and VLA radio data. As a final remark, the coming Square Kilometre Array (SKA) and its existing pathfinder arrays should be able to produce radio weak lensing measurements with similar effectiveness to current optical and NIR work on their own, such that correlating the datasets will radically increase the constraining power of lensing (Bacon et al. 2020). With all this upcoming attention to weak lensing in the radio, we aimed to investigate the specific challenges it brings through this work. The remainder of the paper is organized as follows. In Section 2 we describe the image dataset and stacked catalog. Section 3 presents our method and primary results. In Section 4 we comment on these results and future improvements to them. Finally, Section 5 contains a summary and outlook on the work.

## 2. DATA

The dataset used for this study was a selection of Jansky Very Large Array (VLA) C-band (4-8 GHz) continuum images, mapping extended background galaxy sources in the vicinity of twelve galaxy clusters (Rujopakarn et al., in preparation). The angular resolution in each map ranges from  $0.3'' - 0.5''$  and reach an RMS of  $\approx 2\mu\text{Jy}/\text{beam}$ . The sources were deconvolved from the VLA beam and had major, minor axis measurements extracted via PyBDSF (Mohan & Rafferty 2015). VLA galaxy images reaching sub-arcsecond resolution usually only have a source density of 2-3 sources per square arcminute, which is about ten times too low for doing significant weak lensing work (e.g. compared to Van Waerbeke et al. (2000)). Therefore we elected to "stack" all twelve of the image sets by uniformly superimposing them onto a single abstract cluster origin. This approach of course removed the ability to learn anything about any one background image and the lensing cluster it surrounds on their own, but we hoped to probe relevant thresholds and demonstrate a proof-of-concept for future work. The resultant map of stacked source density is shown in Figure 1. The selection of galaxy clusters used as central targets for mapping is listed in Table 1, and the median, mean redshift to this set is about  $z \sim 0.3$ , with the average redshift to the mapped background sources being roughly  $z \sim 1$  (Rujopakarn et al., in preparation). The format of our stacked catalog is laid out in Table 2.

## 3. ANALYSIS

Now that we have determined our sample data, we can begin searching for a systematic weak lensing signal. Our initial analysis followed the Kaiser & Squires (1993) cluster-inversion technique, outlined in the following subsections.

### 3.1. Deriving ellipticity vectors

We began by deriving the second-moments of each background galaxy's shape. With  $\theta_1$  as the coordinate along a given source's major axis, and  $\theta_2$  along its minor axis; and  $\sigma_1, \sigma_2$  being the respective sizes actually measured along

Column(s)	Description	Units
1	Right Ascension (ICRS) offset	Degrees
2	Declination (ICRS) offset	Degrees
3	Major axis	Arcminutes
4	Minor axis	Arcminutes
5	Position angle	Degrees

**Table 2.** The combined catalog contains 444 sources. RA and Dec "offset" refers to source location with respect to the abstract cluster center origin.

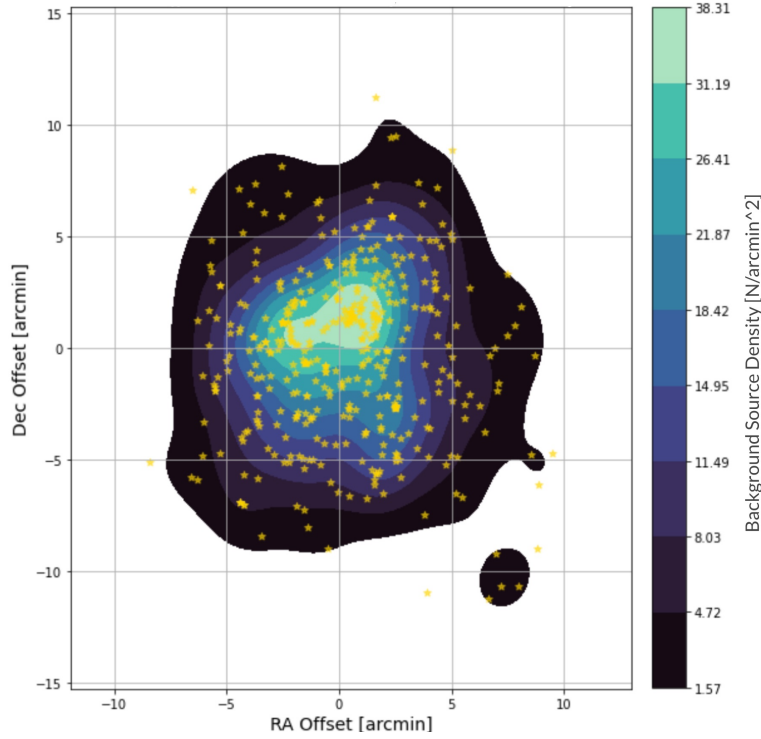


**Figure 1.** Surface number density map of the stacked catalog, with the location of each source galaxy relative to the abstract origin marked in yellow. Note that there are no such markers in the center-most region, as we are attempting to observe the systematic effects of the combined clusters *on* the background galaxies, rather than cluster members themselves. From the color bar values, we can see that the outermost regions show the poor source density indicative of a typical radio image of this type; but the inner 5 contours or so of the stack are definitely within the rich range that is required for significant weak lensing measurements.

each axis, the second-moments are given by (Kaiser & Squires 1993):

$$Q_{11} = \frac{\int d\theta_1 \theta_1^2 e^{-\theta_1^2/2\sigma_1^2}}{\int d\theta_1 e^{-\theta_1^2/2\sigma_1^2}}, \quad Q_{22} = \frac{\int d\theta_2 \theta_2^2 e^{-\theta_2^2/2\sigma_2^2}}{\int d\theta_2 e^{-\theta_2^2/2\sigma_2^2}} \quad (1)$$

Each of these moments was in its source's own frame, which could then be rotated into the unified frame of the stacked image, given the position angle  $\psi$  between the background galaxy's major, minor axes and the shared stack RA, Dec "offset" axes.

$$Q_{xx} = Q_{11} \cos^2(\psi) + Q_{22} \sin^2(\psi), \quad (2)$$

$$Q_{xy} = Q_{11} \cos(\psi) \sin(\psi) - Q_{22} \sin(\psi) \cos(\psi), \quad (3)$$

$$Q_{yy} = Q_{11} \sin^2(\psi) + Q_{22} \cos^2(\psi) \quad (4)$$

We can now write down the desired ellipticity vector for each galaxy. The components of this vector  $\mathbf{e} = e_1, e_2$  are given as ratios of the shape moments, with the following explicit form (Kaiser & Squires 1993):

$$e_1 = \frac{Q_{xx} - Q_{yy}}{Q_{xx} + Q_{yy}}, \quad e_2 = \frac{2Q_{xy}}{Q_{xx} + Q_{yy}} \quad (5)$$

### 3.2. Convoluting vectors into map image

The primary task of this work was to generate a surface mass density map based on the lensed background galaxy ellipticity vectors, from which an estimate of the lensing mass (of the 12 stacked galaxy clusters) could be deduced, shown in Figure 2. In the case of a central polar coordinate system as ours could be represented, the convolution kernel reduced to simply  $\chi = (\cos(2\psi), \sin(2\psi))$  (Kaiser & Squires 1993). Since we have a finitely sampled ellipticity distribution (probed with each background galaxy), we had to use a discrete estimator for the surface mass density map  $\Sigma(\theta)$  as a sum over each source galaxy (Kaiser & Squires 1993).

$$\hat{\Sigma}(\theta) = -\frac{2}{\bar{n}\pi} \sum_{galaxies} \frac{\chi_i(\theta_g - \theta) \cdot e_i(\theta)}{(\theta_g - \theta)^2} = -\frac{2}{\bar{n}\pi} \sum_{galaxies} \frac{e_1(\cos(2\psi)) + e_2(\sin(2\psi))}{|\theta|^2} \quad (6)$$

The "hat" on  $\hat{\Sigma}$  signifies that this distribution is inherently averaged over a finite set of sample points, and  $\bar{n}$  is the surface number density of background galaxies (Kaiser & Squires 1993). Due to such discrete sampling, maps produced in this way are known to suffer from fairly significant noise problems, often referred to as "shot-noise." However, since our target measurement was extracted from just the shared cluster-center region, we could safely filter away much of the sampling-point artifacts and other noise present beyond. We adopted a Gaussian filter  $W$  centered on the stack origin, and found the smoothing radius  $s$  to be most effective at  $s \sim 5$  arcminutes.

$$W(\theta, s) = \left(1 + \frac{|\theta|^2}{2s^2}\right) e^{-\frac{|\theta|^2}{2s^2}} \quad (7)$$

### 3.3. Conversion to physical units

So far by convention, our surface mass density map has been in dimensionless terms, where  $\Sigma = \Sigma_{phys}/\Sigma_{crit}$  (Seitz & Schneider 1995). Thus in order to produce a physical measurement, we had to derive the critical surface mass density and multiply this value with our existing  $\hat{\Sigma}$ . As usual in a cosmological context, the "critical" term has the value required to close the Universe (within your chosen cosmology). We adopted a flat  $\Lambda$ CDM cosmology with the following parameter values, motivated primarily by Dark Energy Survey (DES) 3yr results (Abbott et al. 2021):  $\Omega_m = 0.308$ ,  $\Omega_{rel} = 8.24 \times 10^{-5}$ ,  $\Omega_\Lambda = 0.6911$ ,  $H_0 = 68$  [km/s/Mpc].

The critical surface mass density is given in terms of angular diameter distances to the cluster, to the background galaxies, and between them ( $D_d$ ,  $D_s$ , and  $D_{ds}$  respectively), as (Seitz & Schneider 1995):

$$\Sigma_{crit} = \frac{c^2 D_s}{4\pi G D_d D_{ds}} \quad (8)$$

Based on the information explicitly available in this work, it was more convenient to work in terms of comoving distances, determined as a function of redshift,  $w(z)$ . We therefore calculated comoving distances to the stacked lens, the background galaxies, and separation between them ( $w(0.3) = w_l$ ,  $w(1) = w_g$ ,  $w(0.7) = w_{lg}$ , respectively), using the standard cosmology-dependent equation.

$$w(z) = \frac{c}{H_0} \int_0^z dz' [\Omega_m(1+z')^3 + \Omega_{rel}(1+z')^4 + \Omega_\Lambda]^{-1/2} \quad (9)$$

These comoving distances could then be translated to angular diameter distances by the relation  $D = w(z)/(1+z)$ , and it remained to plug the terms into Eq. 8.

$$\Sigma_{crit} = \frac{c^2 w(1)(1+0.3)(1+0.7)}{4\pi G(1+1)w(0.3)w(0.7)} = \frac{2.21c^2 w(1)}{8\pi G w(0.3)w(0.7)} \Rightarrow 1.972 \times 10^{15} [\text{M}_\odot/\text{Mpc}^2] \quad (10)$$

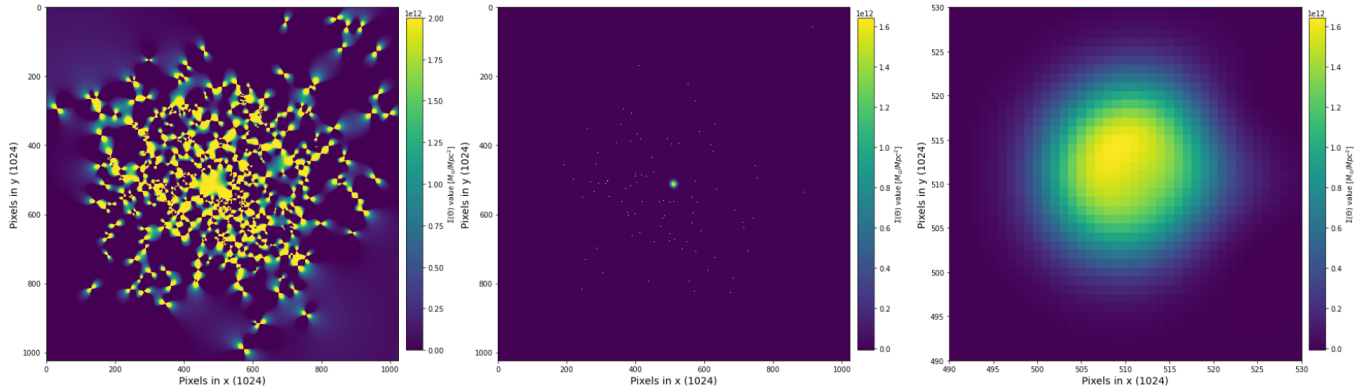


**Figure 2.** (i) The left-hand panel shows the unfiltered  $\hat{\Sigma}_{phys}$  surface mass density map over the full image range, which corresponds to an RA span of  $17.91'$  and Dec span of  $22.45'$  (for a stacked image area of  $402.08$  ( $'$ ) $^2$  or  $0.11$   $\text{deg}^2$ ). The many scattered fluctuations are the contributions from each lensed background galaxy being probed to stitch the map together. Despite the apparent mess, we can still see a strong and consistent positive mass density spike in the central region from the systematic alignment of all the source contributions. (ii) The middle panel shows the same  $\hat{\Sigma}_{phys}$  over the full image range, but with a central Gaussian filter applied ( $s \sim 5'$ ) to isolate the mass signature of the cluster stack. (iii) The right-side panel shows the same filtered  $\hat{\Sigma}_{phys}$  as in (ii), but now zoomed in to view the central region clearly. This sub-field covers about  $41.98''$  in Right Ascension and  $52.62''$  in Declination. The color bar in all all three panels corresponds to the  $\hat{\Sigma}_{phys}$  value, in  $M_{\odot}/\text{Mpc}^2$ .

### 3.4. Mass estimation

Now that we have identified the surface mass density signature of the galaxy cluster stack, we can choose some radius within which to count up an actual mass estimate for the 12 clusters. Choosing  $r \sim 1$  Mpc corresponding to a typical cluster radius, we summed all the pixel values within that range and multiplied by the area of the pixels counted, which gave  $M_{cl.stack} \sim 8.405 \times 10^{14} M_{\odot}$ .

### 3.5. Shot noise uncertainty

The above mass estimate had no sense of its associated uncertainty attached to it yet, so we defined and calculated the shot-noise term that arises from sampling and averaging over a finite ellipticity distribution in the map-making process. This uncertainty measure can be expressed as (Harrison et al. 2020)

$$\mathcal{N} = \frac{\sigma_e^2}{\bar{n}} \quad (11)$$

where  $\sigma_e^2$  is the variance in the background galaxy ellipticity distribution, and  $\bar{n}$  is again the surface number density of these sources in the sample. Carrying out this analysis constrained our lensing mass estimate of the twelve stacked galaxy clusters to  $8.405 \pm 1.092 \times 10^{14} M_{\odot}$ .

### 3.6. Significance analysis

Next we determined a measure of significance for this mass result. We elected to make randomized maps by taking the observed set of ellipticity vectors and randomly reassigning them, followed by re-running the map generation and cluster-mass estimation on each shuffled set. We chose to randomly reassign, rather than randomly regenerate the vector values, so that a physical ellipticity distribution was still being sampled, instead of imposing whatever distribution the random sampler happened to use. This bootstrapping process could then be repeated many times to build a statistical sample of possible mass values to which our observed result could be compared.

Through 800 cycles we saw a Gaussian-like distribution of resultant masses, shown in Figure 3, with a mean value of 1.19, median of 1.10, and standard deviation of 5.01 (each  $[\times 10^{14} M_{\odot}]$ ). These distribution properties translate to a significance of our cluster mass estimate of  $M_{cl.stack} \sim 8.405 \pm 1.092 \times 10^{14} [M_{\odot}]$  at  $1.68 \pm 0.22\sigma$ , which is our primary result. Contracting the whole distribution into rms properties gave a similar result of  $M_{cl.stack} \sim 8.405 \pm 1.092 \times 10^{14} [M_{\odot}]$  at  $1.63 \pm 0.21\sigma_{rms}$ .

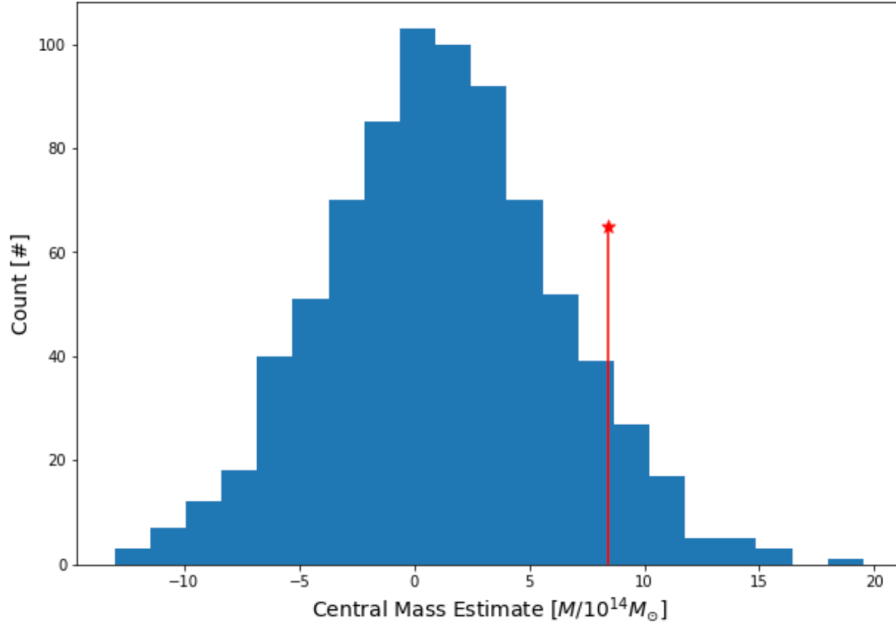


**Figure 3.** Histogram distribution of central cluster-region mass estimates from 800 random shuffles of the observed set of background galaxy ellipticity vectors. The distribution appears to be roughly normal about zero, with a slight positive bias. The red marker indicates where our *observed* cluster stack mass estimate lives in relation to the rest of the distribution.

#### 4. DISCUSSION

The result of our bootstrapped confidence measure was lower than desired, just missing even  $2\sigma$ . However the lensing signal, most clearly seen as the central surface mass over-density on the right side of Figure 2, is well-defined and strongly positive. It did not show any visual signs of artifacts or other noise-induced errors (negative regions, holes, undefined/indeterminable values, etc.), indicating that our stacking method had done a decent job of reinforcing the sparse contribution of each individual background galaxy shear into a systematic signal. Furthermore, the mass estimate we obtained is of the same order as typical measurements of multiple clusters or small superclusters, which aligns with our sample size of 12 galaxy-clusters (e.g. Chon, Gayoung et al. 2015, and therein).

##### 4.1. Improved analyses

The next step in our analysis will be to implement an aperture-mass statistic (Schneider 1996), which should be more well suited to the specific cluster-lensing profile. For an example of this method in practice, see Fong et al. (2019). This algorithm will help refine our mass estimation and strengthen its confidence by identifying the target signal more directly.

If the requisite data are available, we would like to investigate the direct probes of *intrinsic* background galaxy ellipticity in practice, and examine if such radio polarimetry, kinematic data can indeed reduce the statistical uncertainty and shot-noise. Likewise, we hope to compare our results with established optical lensing and virial analyses, respectively to check the accuracy of our method and see if any dark matter distributions or constraints can be observed.

##### 4.2. Sample refinement

If the Schneider (1996) method succeeds in bringing the significance over  $3\sigma$ , we will then examine how many source galaxies can be arbitrarily removed from the stack while still maintaining a  $3\sigma$  detection; with the goal of setting a relevant threshold for how much stacking is necessary to get a weak lensing measurement from current radio data. Conversely if the optimized algorithm alone is not enough, we can then see how extreme the stacking must be in order to achieve the desired confidence. Regardless of the amount of data stacking though, we are additionally implementing a deeper screen for cluster-member galaxies which have intruded into the background sample, obfuscating the weak

lensing signal. This will be somewhat mitigated as some of the radio images were not centered on their respective clusters (Rujopakarn et al., in preparation), but some cluster radio sources are probably present in the current catalogs.

## 5. CONCLUSIONS

We have presented preliminary results towards the first detection of "small-scale" weak gravitational lensing using only radio data (cluster-driven or smaller, rather than large-scale-structure based cosmic shear). Our current method used a stacked catalog of many high-resolution radio continuum maps of background sources surrounding 12 galaxy clusters, in the hopes of reaching the requisite source number density for a statistically significant lensing analysis. This study will be improved with a more suitable aperture-mass statistic (Schneider 1996), in place of the Kaiser & Squires (1993) cluster-inversion technique. To help motivate this work and put it in a legitimate context, we mentioned a few powerful features that radio observations can bring to the table in weak lensing; as well as mentioning some established and future works in this area. Namely, recall that there may be a critical window in certain radio data on the *intrinsic* (unlensed) background ellipticity distribution (Stil et al. 2009; Wright 1974), which is usually unknown and assumed to be random en-large (e.g. Seitz & Schneider 1995). Additionally, we noted the observational and pipeline differences between radio interferometers and optical/NIR telescopes, such that correlating data from each could drastically reduce systematic uncertainty in weak lensing studies, with SuperCLASS as a current survey example (Harrison et al. 2020). With the coming next-generation of radio arrays, like ngVLA (Casey et al. 2018; Carilli et al. 2018) and SKA (Bacon et al. 2020), we hope that this preliminary work in radio lensing can help set the foundation for unprecedented constraining power in the future.

## ACKNOWLEDGEMENTS

AG thanks M. Lacy and A. Sajina for dedicated mentorship and guidance, as well as NSF and NRAO-REU program for supporting this work. AG, ML acknowledge W. Rujopakarn for offering the high-resolution VLA data, in addition to L. King, K. Nyland for consultation.

## REFERENCES

- Abbott, T. M. C., et al. 2021.  
<https://arxiv.org/abs/2105.13549>
- Bacon, D. J., Battye, R. A., Bull, P., et al. 2020,  
 Publications of the Astronomical Society of Australia, 37,  
 e007, doi: [10.1017/pasa.2019.51](https://doi.org/10.1017/pasa.2019.51)
- Battye, R. A., Brown, M. L., Casey, C. M., et al. 2020,  
 Monthly Notices of the Royal Astronomical Society, 495,  
 1706–1723, doi: [10.1093/mnras/staa709](https://doi.org/10.1093/mnras/staa709)
- Blain, A. W. 2002, ApJL, 570, L51, doi: [10.1086/341103](https://doi.org/10.1086/341103)
- Brown, M. L., & Battye, R. A. 2011, MNRAS, 410, 2057,  
 doi: [10.1111/j.1365-2966.2010.17583.x](https://doi.org/10.1111/j.1365-2966.2010.17583.x)
- Carilli, C., McKinnon, M., Ott, J., et al. 2018, Next  
 Generation Very Large Array Memo No. 5 Science  
 Working Groups Project Overview
- Casey, C. M., Narayanan, D., Carilli, C., et al. 2018,  
 Science with an ngVLA: Imaging Cold Gas to 1 kpc  
 Scales in High-Redshift Galaxies with the ngVLA.  
<https://arxiv.org/abs/1810.08258>
- Chang, T.-C., Refregier, A., & Helfand, D. J. 2004, The  
 Astrophysical Journal, 617, 794, doi: [10.1086/425491](https://doi.org/10.1086/425491)
- Chon, Gayoung, Böhringer, Hans, & Zaroubi, Saleem. 2015,  
 A&A, 575, L14, doi: [10.1051/0004-6361/201425591](https://doi.org/10.1051/0004-6361/201425591)
- Demetroullas, C., & Brown, M. L. 2017, Monthly Notices of  
 the Royal Astronomical Society, 473, 937,  
 doi: [10.1093/mnras/stx2366](https://doi.org/10.1093/mnras/stx2366)
- Fong, M., Choi, M., Catlett, V., et al. 2019, MNRAS, 488,  
 3340, doi: [10.1093/mnras/stz1882](https://doi.org/10.1093/mnras/stz1882)
- Harrison, I., Brown, M. L., Tunbridge, B., et al. 2020,  
 Monthly Notices of the Royal Astronomical Society, 495,  
 1737, doi: [10.1093/mnras/staa696](https://doi.org/10.1093/mnras/staa696)
- Heymans, C., Tröster, T., Asgari, M., et al. 2021,  
 Astronomy Astrophysics, 646, A140,  
 doi: [10.1051/0004-6361/202039063](https://doi.org/10.1051/0004-6361/202039063)
- Kaiser, N., & Squires, G. 1993, ApJ, 404, 441,  
 doi: [10.1086/172297](https://doi.org/10.1086/172297)
- Mohan, N., & Rafferty, D. 2015, PyBDSF: Python Blob  
 Detection and Source Finder. <http://ascl.net/1502.007>
- Morales, M. F. 2006, ApJL, 650, L21, doi: [10.1086/508614](https://doi.org/10.1086/508614)
- Oguri, M., Takada, M., Okabe, N., & Smith, G. P. 2010,  
 MNRAS, 405, 2215,  
 doi: [10.1111/j.1365-2966.2010.16622.x](https://doi.org/10.1111/j.1365-2966.2010.16622.x)
- Schneider, P. 1996, MNRAS, 283, 837,  
 doi: [10.1093/mnras/283.3.837](https://doi.org/10.1093/mnras/283.3.837)
- Seitz, C., & Schneider, P. 1995, A&A, 297, 287.  
<https://arxiv.org/abs/astro-ph/9408050>

Stil, J. M., Krause, M., Beck, R., & Taylor, A. R. 2009, *The Astrophysical Journal*, 693, 1392, doi: [10.1088/0004-637x/693/2/1392](https://doi.org/10.1088/0004-637x/693/2/1392)

Taylor, E. N., Cluver, M. E., Duffy, A., et al. 2020, *MNRAS*, 499, 2896, doi: [10.1093/mnras/staa2648](https://doi.org/10.1093/mnras/staa2648)

Van Waerbeke, L., Mellier, Y., Erben, T., et al. 2000, *A&A*, 358, 30. <https://arxiv.org/abs/astro-ph/0002500>

Wright, M. C. H. 1974, *Mapping Neutral Hydrogen in External Galaxies*, ed. G. L. Verschuur, K. I. Kellermann, & V. van Brunt, 127, doi: [10.1007/978-3-642-96178-6\\_11](https://doi.org/10.1007/978-3-642-96178-6_11)